Feature Extraction from Interferograms for Phase Distribution Analysis

Torsten Merz[a], Dietrich Paulus[b], and Heinrich Niemann

Universität Erlangen-Nürnberg, Lehrstuhl für Mustererkennung
Martensstr. 3, 91058 Erlangen, Germany

ABSTRACT

In several applications of interferogram analysis, e.g. automated nondestructive testing, it is necessary to detect irregular interference phase distributions or to compare interference phase distributions with each other. For that purpose it is useful to represent the essential information of phase distributions by characteristic features. We propose features which can be extracted both from interferograms as well as from phase distributions. For feature extraction we developed new image processing methods analyzing the local structure of gray-level images. The feature extraction is demonstrated with examples of a cantilever beam and a pressure vessel using holographic interferometry. Finally we show the use of the features for defect detection and phase distribution comparison.

Keywords: holographic interferometry, feature extraction, image processing, fringe analysis, nondestructive testing

1. INTRODUCTION

Interference effects occur when two mutually coherent waves fields are superposed. By analyzing the spatial intensity distribution (interference pattern) of the superposition, we have means to get information about the spatial interference phase difference distribution (shortly phase distribution). So it is possible to compare wave fields with each other. Using one wave as a reference and the other as an object wave, we can get information about an object which introduces a phase variation by analyzing the resulting interference pattern. Phase variations can be introduced due to variation of light path length, e.g. by displacing a reflecting surface, or due to variation of refractive index, e.g. by changing the density in a gas. In case of objects producing specular wave fields, we can only compare wave fields with introduced phase variations which are smooth compared to the speckle producing interference. This is possible e.g. with holographic interferometry, where the wave fields of two states of the same object are compared by storing one in a hologram.

Our goal in interferogram analysis is to extract the essential information about the underlying phase distribution from both interferograms and phase distributions. Of course there is a loss of information and robustness by analyzing only one interferogram instead of the phase distribution which can be reconstructed using additional information. Nevertheless, for many applications the maximal information extracted from a single interferogram is sufficient.

Features of any pattern should have the property to represent the essential information which is relevant for a given analysis task. Here features have to be independent of background intensity, fringe contrast, and speckle effects. In addition, the features should be independent of an arbitrary phase offset (i.e. an unknown reference phase), as on the one hand it is not possible to reconstruct the absolute phase from interferograms without any further information and on the other hand the absolute phase is unstable due to vibrations or e.g. due to inexact hologram repositioning. In most cases of qualitative interferogram analysis, the influence of the reference phase has not been considered yet. For illustration of the effect see Fig. 1 where two one-dimensional interference patterns are shown resulting from the same phase distribution but with different reference phases.

Further author information –
E-mail: merz@informatik.uni-erlangen.de[a], paulus@informatik.uni-erlangen.de[b]
WWW: http://www5.informatik.uni-erlangen.de

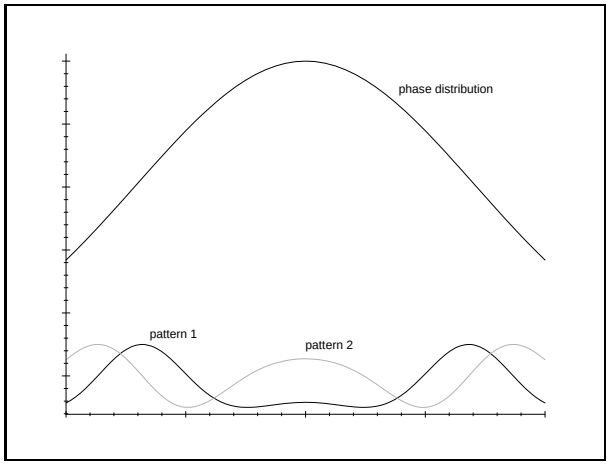

Figure 1. Dependence of interference patterns from different reference phases

2. EXPERIMENTAL DESCRIPTION

For the verification of the developed methods we use two experimental setups: on the one hand an aluminum cantilever beam bent by a shearing force and on the other hand an aluminum pressure vessel elastically deformed by pressure, both measured in a standard holographic setup (Fig. 2). The holographic recording material is a photopolymer which makes wet chemical processing and hologram repositioning superfluous, the hologram can be viewed immediately after exposure. After having recorded the wave field belonging to one object state, a phase variation is introduced and the corresponding interferogram can be viewed in real time (real-time holographic interferometry). A conventional piezo-electric transducer is used for temporal phase-shifting of the reference wave. Interferograms are recorded with a standard black and white CCD-camera and processed with a standard Pentium PC.

The cantilever beam experiment enables easy quantitative verification of the experimental results as an analytical description of the surface deflection exists:[1]

$$d(x) = \frac{F}{Ewh^3}\left(6\,lx^2 - 2x^3\right)$$

where F is the shearing force, E the modulus of elasticity, w the beam width, h the beam thickness, l the beam length, and x the distance from the fixation.

Due to the small angle between incident and reflected light in the arrangement of the optical setup, the influence of the sensitivity vector can be neglected. Thus the one-dimensional phase distribution is given by:[2]

$$\delta(x) = \frac{4\pi}{\lambda} d(x)$$

In a first experiment we measured the bending of the cantilever beam using holographic interferometry as described in section 3 and compared it with the analytical solution (Fig. 3). Since the solution shows high correspondence with the theoretical values, we considered the accuracy as sufficient for the following experiments.

The pressure vessel is used to produce more complex interference patterns and to demonstrate the application of the proposed methods in nondestructive testing. It is prepared with an artificial subsurface flaw which can be detected using the proposed features as shown in section 5.

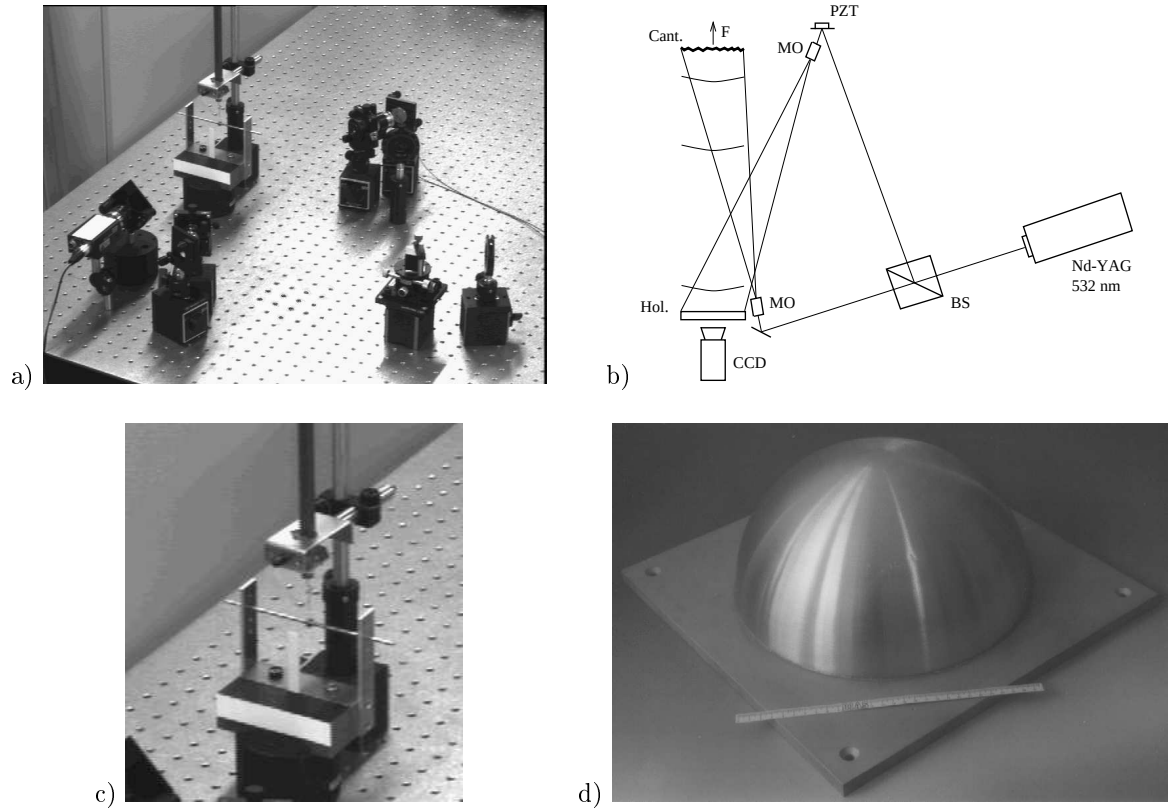

Figure 2. a) Setup of the cantilever beam experiment, b) holographic interferometer: BS=beam splitter, MO=microscope objective, PZT=piezo-electric transducer, c) cantilever beam, d) investigated pressure vessel

3. FEATURE DEFINITION

In holographic interferometry the intensity distribution of interferograms can be described by the following expression:[2]

$$I(x,y) = a(x,y) + b(x,y)\,\cos(\delta(x,y) + \Phi_R) \tag{1}$$

where $\delta(x,y)$ is the underlying phase distribution, Φ_R the reference phase and $a(x,y)$ and $b(x,y)$ are the additive and multiplicative distortions (background intensity, speckle noise, varying fringe visibility).

In case of having a sequence of interferograms of continuously deforming objects or with continuously varying reference phase, it is possible to eliminate the additive and multiplicative distortions for each interferogram of the sequence.[3] The normalized intensity is then given by:

$$\tilde{I}(x,y) = \cos(\delta(x,y) + \Phi_R)$$

Using four interferograms $I_n(x,y)$ belonging to the same object state recorded with unknown but constant phase shift $\Delta\Phi$ of the reference wave, it is possible to reconstruct the phase distribution modulo 2π by solving equation 1 with $\Phi_{R_n} = n\Delta\Phi$.[2] In order to get a continuous phase distribution, the wrapped phase can be demodulated using e.g. the path-independent algorithm described in.[2]

We have four kinds of patterns representing phase information: interferograms, normalized interferograms, wrapped phase distributions, and demodulated phase distributions. It will be shown in the following that under certain conditions there exist features of the same kind which can be extracted from all four kinds of patterns and

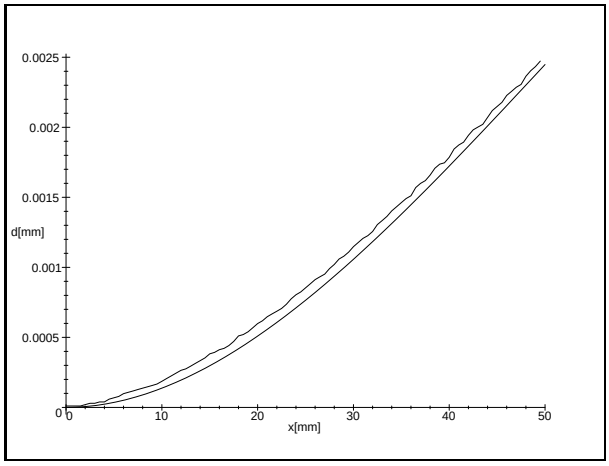

Figure 3. Bending of the cantilever beam calculated from phase distribution compared with analytical solution

which are independent of the unknown reference phase. These features are calculated using only spatially local information. So it is possible to handle discontinuities like wrapped phases by skipping regions in which discontinuities appear. In these regions there is no phase information available, of course, but in many cases it is possible either to reject this information or to interpolate from neighboring features.

We propose two features with these properties: fringe density $\rho(x,y)$ and fringe direction $\alpha(x,y)$ – the denotation will be clear later on. In the following theorem the conditions, the properties and the way how to calculate these features are summarized in case of having a phase distribution function $\delta(x,y)$ or a corresponding normalized intensity function $\tilde{I}(x,y)$:

THEOREM 1.

$$\forall (x_o,y_o) \textit{ for which } \delta(x,y) \textit{ in a neighborhood of } (x_o,y_o) \textit{ is continuously differentiable and } |\tilde{I}(x_o,y_o)| < 1 :$$

$$\rho(x_o,y_o) = |\operatorname{grad}\delta(x_o,y_o)| = |\operatorname{grad}[\delta(x_o,y_o)+\Phi_R]| = |\operatorname{grad}[\arccos\tilde{I}(x_o,y_o)]|$$

$$\alpha(x_o,y_o) = \begin{cases} \arctan\frac{\operatorname{grad}_y\delta(x_o,y_o)}{\operatorname{grad}_x\delta(x_o,y_o)} = \arctan\frac{\operatorname{grad}_y[\delta(x_o,y_o)+\Phi_R]}{\operatorname{grad}_x[\delta(x_o,y_o)+\Phi_R]} = \arctan\frac{\operatorname{grad}_y[\arccos\tilde{I}(x_o,y_o)]}{\operatorname{grad}_x[\arccos\tilde{I}(x_o,y_o)]} & : \operatorname{grad}_x \neq 0 \\ \frac{\pi}{2} & : \operatorname{grad}_x = 0 \wedge \operatorname{grad}_y \neq 0 \end{cases}$$

Thus gradient calculation from wrapped or demodulated phase distributions or from the arcus cosine of normalized interferograms is the basic function for feature extraction. It is also possible to estimate fringe density and fringe direction from a single interferogram if the underlying phase distribution can be approximated locally by a plane:

THEOREM 2.

if $\exists$ *a quadratic region* $B = \{(x,y)|x_1 \leq x \leq x_2 \wedge y_1 \leq y \leq y2\}$ *with* $(x_o,y_o) \in B$ *and following properties:*
$\forall\,(x,y) \in B$ *holds:* $\operatorname{grad}\delta(x,y) = \boldsymbol{const} \neq \mathbf{0} \wedge a(x,y) = const \wedge b(x,y) = const \neq 0$
$\wedge\ \exists$ *ridge-line of* I *with point* $\in B \wedge \exists$ *ravine-line of* I *with point* $\in B$

then $\rho(x_o,y_o) = \frac{\pi}{l}$ *with*
$l =$ *distance between ridge-line and adjacent ravine-line*
$\alpha(x_o,y_o) =$ *angle between y-axis and ridge-line*

Thus it is possible to calculate the same kind of features of all types from a single interferogram as from phase distributions by estimating the local fringe density and fringe direction in the gray-level image – hence the feature denotation. Many common methods for interferogram analysis are based on the analysis of fringe structure, especially qualitative analysis methods for nondestructive testing[4,5] or phase evaluation methods based on fringe counting, but one has to keep in mind the assumptions made about the phase distribution. As the proof of both theorems is straightforward (requires substitution, use of gradient calculation laws, and properties of cosine function), it is left out here.

FOR all j,k	
	estimate gradient vector $\boldsymbol{v}_{jk}$ (see Theorem 3) from phase distribution
FOR all j,k	
	calculate mean gradient vector (n-times): $\boldsymbol{v'}_{jk} := \sum_{\mu=-m}^{m} \sum_{\nu=-m}^{m} \boldsymbol{v}_{j+\mu,k+\nu}$
	calculate fringe direction: $\alpha_{jk} := \arctan(v'_{jk_y}, v'_{jk_x}) \bmod \pi$
	calculate fringe density: $\rho_{jk} := \sqrt{{v'_{jk_x}}^2 + {v'_{jk_y}}^2}$

Figure 4. Algorithm for calculation of fringe direction and fringe density from phase distributions

4. FEATURE EXTRACTION

As we have shown in the last section we have to estimate gradients of two dimensional discrete scalar fields. This can be done by least-squares fitting of a plane $z = ax + by + c$ to the pattern f_{jk} within a quadratic region (plane window) and calculating the gradient of the plane:[6,7]

THEOREM 3.

let f_{jk} be a sampled pattern of the continuously differentiable function $f(x,y)$ then:

$$\operatorname{grad} f_{jk} \approx (a_{jk}, b_{jk})^T \quad \textit{with}$$

$$a_{jk} = \gamma \sum_{\mu=-m}^{m} \sum_{\nu=-m}^{m} f_{j+\mu,k+\nu}\,\mu \quad \textit{and} \quad b_{jk} = \gamma \sum_{\mu=-m}^{m} \sum_{\nu=-m}^{m} f_{j+\mu,k+\nu}\,\nu \quad \textit{and} \quad \gamma = \frac{3}{m(m+1)(2m+1)^2}$$

An important parameter for gradient estimation accuracy with noisy patterns is the size m of the plane window. If we know the maximal surface curvature of the scalar field, it is possible to get an estimation for a suitable maximal window size. In addition, if we assume that the scalar field is *smooth* we can smooth the gradient vectors nearly without loss of information but with considerable improvement of signal to noise ratio. The selection of suitable parameter values is e.g. in case of the cantilever beam no problem as there exists an analytical description of possible phase distributions. In Fig. 4 an algorithm using Theorem 3 for calculation of fringe direction and fringe density from continuous phase distributions is shown. The number of iterations n for smoothing the gradient vector depends on the noise power of the pattern (typical values for n between 1 and 4).

4.1. Feature Extraction based on Theorem 1

We use the cantilever beam experiment to compare features extracted from measured patterns with theoretically expected features. The accuracy of the measured bending curve already was discussed in section 2. In Fig. 5a) the measured phase distribution is shown (phase corresponds to brightness of gray-level), in Fig. 5b) the features are visualized in a needle image (fringe direction=direction of needle, fringe density=length of needle) and in Fig. 5c) the calculated and expected fringe density are shown.

Features from wrapped phase distributions are extracted in the same way except that we have to skip points with discontinuities inside the plane window. Skipped regions can be interpolated by repeated smoothing of the gradient vector. Of course this only works properly for phase distributions with low fringe density compared to the region size m. Alternatively a simple local phase unwrapping algorithm could be used to unwrap only the phase within the plane window. In Fig. 6 the results of the feature extraction from the wrapped phase distribution of the cantilever beam without phase unwrapping are shown.

The calculation of features from normalized interferograms is similar to the algorithm in Fig. 4, but the mean gradient vectors are calculated with the algorithm shown below in Fig. 10. There is also a discontinuity problem, namely regions around $|\tilde{I}(x,y)| = 1$. These regions are treated in the same way as described for feature extraction from wrapped phase distributions. In Fig. 7 the results of the feature extraction from the arcus cosine distribution of the cantilever beam are shown. The normalized interferogram is calculated using interferograms from ten different loadings.

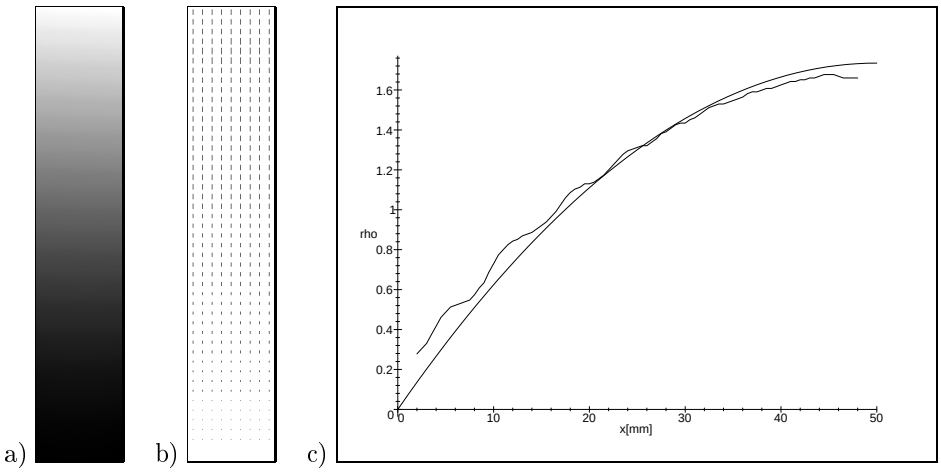

Figure 5. Feature extraction from phase distribution: a) phase image, b) needle image showing calculated fringe direction and fringe density, c) expected and calculated fringe density

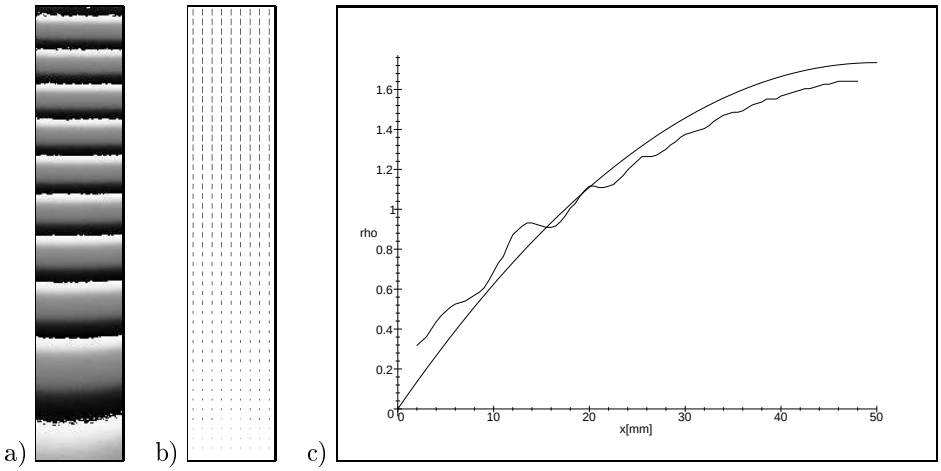

Figure 6. Feature extraction from wrapped phase distribution: a) wrapped phase image, b) needle image showing calculated fringe direction and fringe density, c) expected and calculated fringe density

4.2. Feature Extraction based on Theorem 2

Estimating local frequency and local direction of gray-level image structures is a common problem in image processing especially for texture analysis.[8,9] But conventional methods do not work properly for interferograms as we have to consider speckle influences and greatly varying fringe densities. Therefore we have developed a new image processing method which makes use of the property that fringe direction changes slowly within a region compared to speckle structure. The basic idea behind the algorithm is to calculate several gradient direction images $g_{jk}^{(i)}$ with n different plane window sizes m_i from a sampled interferogram (Theorem 3) and to use the direction information for estimation of fringe direction and fringe width. In a first step a common gradient direction image g_{jk} is put together from the different gradient direction images $g_{jk}^{(i)}$ according to a direction homogeneity criterion and in a second step an improved gradient direction image is put together according to the fringe width estimated from the first gradient direction image (Fig. 8). The algorithm is described in detail in Fig. 9, 10 and 11.

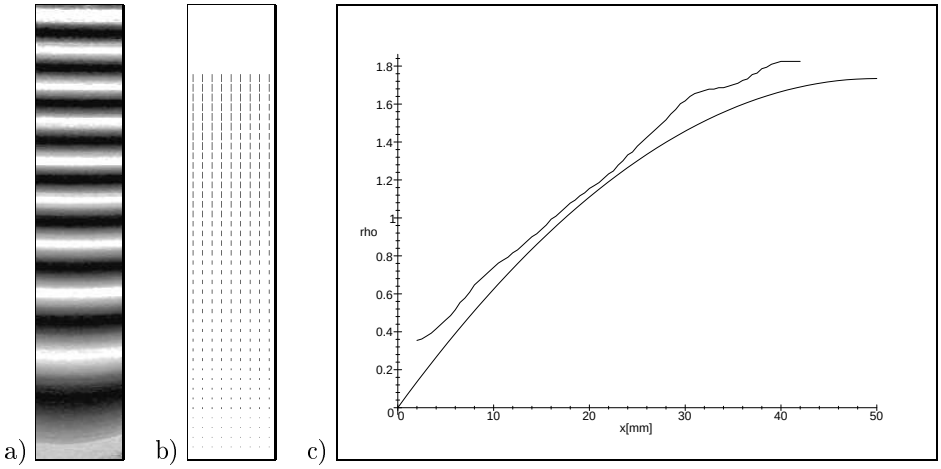

Figure 7. Feature extraction from arcus cosine distribution: a) arcus cosine image, b) needle image showing calculated fringe direction and fringe density, c) expected and calculated fringe density

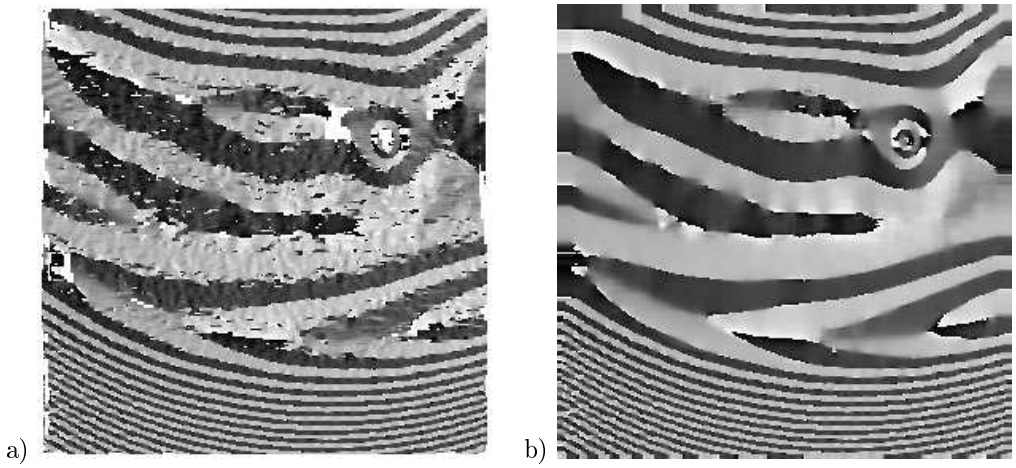

Figure 8. a) First gradient direction image calculated from Fig. 13a, b) improved direction image

calculate gradient direction images $g_{jk}^{(i)}$ with n different plane window sizes $m_1 < m_i < m_n$ (see Theorem 3)			
FOR $i := 1$ to n			
	calculate mean fringe direction vectors $\boldsymbol{v'}_{jk}$ (see Fig. 10)		
	FOR all j,k		
		IF	$\lvert \sum_{\mu=-m}^{m} \sum_{\nu=-m}^{m} \boldsymbol{v'}_{j+\mu,k+\nu} \rvert > \theta_h$
		THEN	direction is homogeneous at jk
initialize gradient direction image: $\forall j,k : g_{jk} := no\,direction$			
FOR all j,k			
	FOR $i := n$ down to 1		
		IF	direction from image $g_{jk}^{(i)}$ is homogeneous
		THEN	$g_{jk} := g_{jk}^{(i)}$
calculate fringe width w_{jk} and fringe direction α_{jk} from g_{jk} (see Fig. 11)			
initialize improved gradient direction image: $\forall j,k : g_{jk} := g_{jk}^{(n)}$			
FOR all j,k			
	FOR $i := 1$ to n		
		IF	$2m_i < w_{jk}$
		THEN	$g_{jk} := g_{jk}^{(i)}$
calculate fringe width w_{jk} and fringe direction α_{jk} from g_{jk} (see Fig. 11)			
FOR all j,k			
	calculate fringe density: $\rho_{jk} := \frac{\pi}{w_{jk}}$		

Figure 9. Algorithm for calculation of fringe direction and fringe density from single interferograms

FOR all j,k	
	calculate fringe direction from gradient direction: $\alpha_{jk} := g_{jk} \bmod \pi$
	calculate unit vector with direction $2\alpha_{jk}$: $\boldsymbol{v}_{jk} := (\cos(2\alpha_{jk}), \sin(2\alpha_{jk}))^T$
FOR all j,k	
	calculate mean direction vector (n-times): $\boldsymbol{v'}_{jk} := \sum_{\mu=-m}^{m} \sum_{\nu=-m}^{m} \boldsymbol{v}_{j+\mu,k+\nu}$
	calculate fringe direction: $\alpha_{jk} := \frac{\arctan(v'_{jk_y}, v'_{jk_x})}{2}$

Figure 10. Algorithm for calculation of fringe direction images from gradient direction images

calculate mean fringe direction image α_{jk} (see Fig. 10)
FOR all j,k
calculate fringe width w_{jk}: move along a line through jk with direction α_{jk} and $\alpha_{jk} + \pi$ until reaching two points where gradient direction changes more than threshold θ_g; w_{jk}:=distance between points
smooth fringe width image w_{jk} by mean filtering

Figure 11. Algorithm for calculation of fringe width and fringe direction from gradient direction images

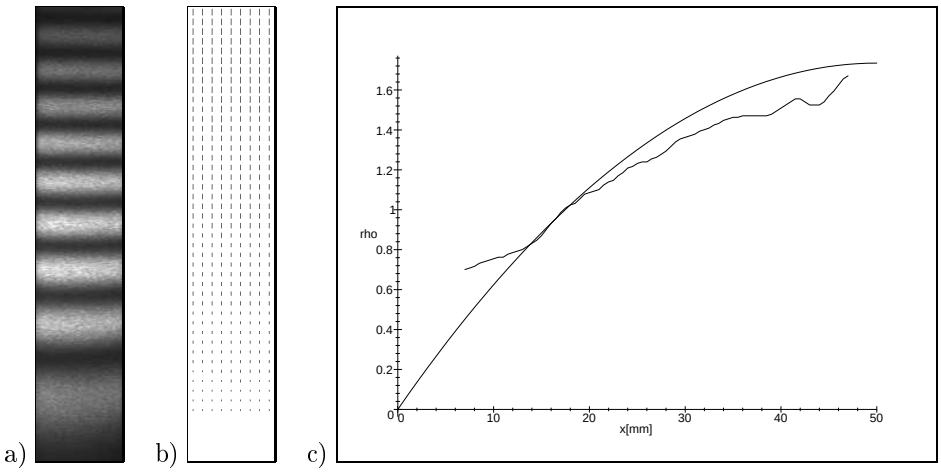

Figure 12. Feature extraction from single interferogram: a) interferogram, b) needle image showing calculated fringe direction and fringe density, c) expected and calculated fringe density

Fig. 12 shows the results of the feature extraction from a single interferogram of the cantilever beam. In order to demonstrate also the accuracy of the fringe direction calculation, we used interferograms of the pressure vessel, which produces more complex interference patterns. The results of the feature extraction from a single interferogram and from the measured phase distribution are shown in Fig. 13.

Comparing the results of the feature extraction from the different input patterns, one notices that the feature values differ more or less although theoretically they should be the same. This is on the one hand due to different noise levels of the input patterns and different smoothing techniques, and on the other hand due to patterns which do not comply with the assumptions made about the phase distribution.

5. FEATURE ANALYSIS

In the previous sections we described how to extract suitable features for phase distribution analysis, now we show how to use these features. A possible use is pattern classification with statistical methods or artificial neural networks where the membership of patterns to a certain class is learned using characteristic features. In both cases we need a representative sample containing enough samples of possible patterns which have to be recognized. Due to the great variety of different interference patterns and difficult experimental realization it is difficult to produce a representative sample. Therefore the sample is often produced by simulation. Nevertheless there are successful applications in qualitative interferogram analysis, e.g. defect detection in nondestructive testing with artificial neural networks.[2]

For demonstration of the use of the extracted features we propose a simple method for defect detection which does not need any sample, the necessary knowledge is formulated explicitly in an algorithm. The algorithm shown in Fig. 14 determines the centers of nearly circular interference patterns. Such patterns often appear in the region of subsurface flaws. There are four parameters ($i_{\max}$, r, θ_α, and θ_ρ) which have to be adjusted using either expert knowledge or a representative sample. The algorithm was successfully used to detect the subsurface flaw of the pressure vessel (Fig. 13).

Finally the features can be used for comparison of phase distributions. The local deviation d_{jk} between two phase distributions δ and δ' can be evaluated simply by vector subtraction:

$$d_{jk} = \left\| \rho_{jk} \begin{pmatrix} \cos(2\alpha_{jk}) \\ \sin(2\alpha_{jk}) \end{pmatrix} - \rho'_{jk} \begin{pmatrix} \cos(2\alpha'_{jk}) \\ \sin(2\alpha'_{jk}) \end{pmatrix} \right\|$$

Having a parametric model function which describes the phase distribution this measure can be used in an iterative control cycle for parameter estimation in an inverse problem. We currently develop a method for detection of elliptic inclusions in pressure vessels using a hybrid technique of interferometric measurement and deformation simulation.[5]

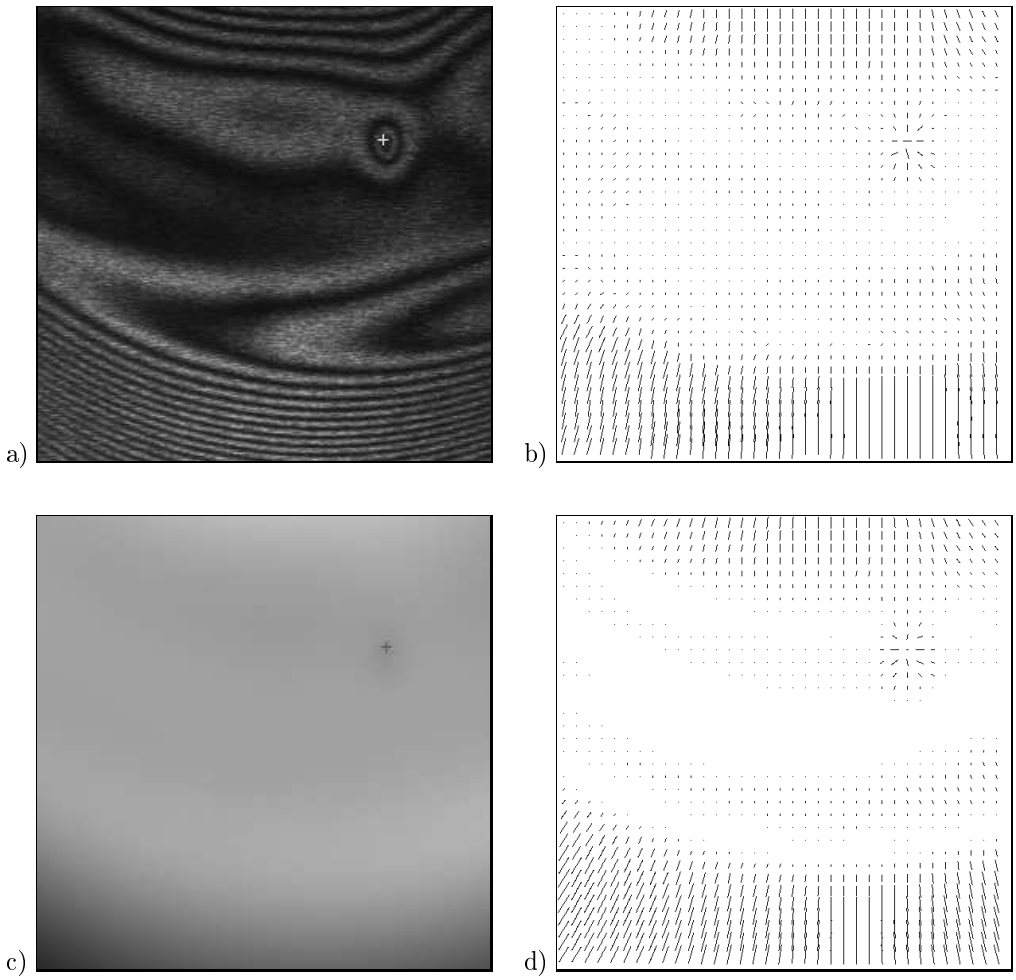

Figure 13. a) Interferogram of the pressure vessel with identified circular pattern (subsurface flaw), b) needle image showing fringe direction and fringe density calculated from single interferogram, c) corresponding phase distribution, d) needle image calculated from phase distribution

6. CONCLUSION

We proposed two kind of features which contain maximal information about phase distributions: fringe density and fringe direction. They can be extracted both from interferograms as well as from phase distributions and they are independent of the reference phase. We developed new image processing methods for analyzing the local direction and local frequency of gray-level image structures. For each feature extraction method we have shown results which are compared with the analytical solution of the cantilever beam experiment. The best results we obtain with features from continuous phase distributions. If very accurate results are required one should use reconstructed phase distributions for analysis. Nevertheless in many cases especially in qualitative interferogram analysis the accuracy of the other feature extraction methods, which do not need any phase-shifting, is sufficient, if the prerequisites of the algorithms are considered. Finally we have shown how these features can be used for defect detection and phase distribution comparison.

ACKNOWLEDGMENTS

The authors wish to thank the Bremen Institute of Applied Beam Technology (BIAS) for producing the interferograms of the pressure vessel and the Fraunhofer Institute for Integrated Circuits for helping to set up the cantilever beam experiment. This work is financed by the Deutsche Forschungsgemeinschaft (DFG).

initialize cluster image: $\forall j,k : c_{jk} := 0$			
FOR all j,k			
	initialize counter: $n := 0$		
	FOR $i := 0$ to $i_{\max} - 1$		
		calculate test coordinates on circle around jk with radius r: $\mu := \lfloor r \cos(\frac{i}{i_{\max}} 2\pi) + j + \frac{1}{2} \rfloor$ $\nu := \lfloor r \sin(\frac{i}{i_{\max}} 2\pi) + k + \frac{1}{2} \rfloor$	
		calculate difference angle: $\Delta\alpha := \lvert \alpha_{\mu\nu} - \frac{i}{i_{\max}} 2\pi \rvert$	
		IF	$\Delta\alpha > \frac{\pi}{2}$
		THEN	$\Delta\alpha := \pi - \Delta\alpha$
		IF	difference angle admissible and fringe density sufficient: $\Delta\alpha < \theta_\alpha \wedge \rho_{\mu\nu} > \theta_\rho$
		THEN	$n := n + 1$
	IF	$n = i_{\max}$	
	THEN	mark possible center of circular pattern: $c_{jk} := 1$	
generate list of contours from cluster image (0=background, 1=foreground)			
FOR all contours in list			
	calculate center of gravity from contour		

Figure 14. Algorithm for detection of circular patterns from fringe direction and fringe density

REFERENCES

1. R. Fenner, *Engineering Elasticity*, Ellis Horwood, Chichester, 1986.
2. T. Kreis, *Holographic Interferometry*, Akademie Verlag, Berlin, 1996.
3. T. Merz, D. Paulus, and H. Niemann, "Line Segmentation for Interferograms of Continuously Deforming Objects," in *International Conference on Experimental Mechanics: Advances and Applications*, F. Chau and C. Lim, eds., vol. 2921, pp. 325–330, SPIE, 1997.
4. U. Mieth, W. Osten, and W. Jüptner, "Knowledge Assisted Fault Detection Based on Line Features of Skeletons," in *Fringe '93*, J. W. and W. Osten, eds., pp. 367–373, Akademie Verlag, (Berlin), October 1993.
5. T. Merz and F. Elandaloussi, "Automatic Fringe Analysis for Model Based Flaw Recognition," in *Fringe'97*, W. Jüptner and W. Osten, eds., vol. 3, pp. 132–135, Akademie Verlag, (Berlin), 1997.
6. H. Niemann, *Pattern Analysis and Understanding*, Springer, Berlin, second ed., 1990.
7. R. M. Haralick and L. G. Shapiro, *Computer and Robot Vision*, vol. 1, Addison–Wesley, Reading, MA, 1992.
8. B. Jähne, *Digital Image Processing*, Springer, Berlin, 1991.
9. G. Granlund, *Signal Processing for Computer Vision*, Kluwer Academic Publishers, Dordrecht, 1995.